Design of a Cylindrical Flexure Jointed Stewart Platform for Aligning the Condenser in an X-ray Microscope

Sung-hoon Kang[1,#], Dong Woo Kang[1], Dae Gab Gweon[1], Gwon-Ha Yoon[2] and Jin Young Min[3]

1 Department of Mechanical Engineering, KAIST, Guseong-dong, Yuseong-gu, Daejeon, South Korea
2 Department of Radiology, Wonkwang University School of Medicine, Jeonbuk, South Korea
3 LISTEM Co. Ltd., Chungchun-2-dong, Bupyeong-gu, Incheon 403-032, Korea
Corresponding Author / E-mail: kangdongggg@kaist.ac.kr, TEL: +82-42-869-8763, FAX: +82-42-869-8763

KEYWORDS : Optics alignment, Flexure, Stewart platform, X-ray microscope

This paper proposes a new type of six degree-of-freedom fine positioner that can be used to align the condenser in X-ray microscopy precisely. The new concept was based on the requirements for an X-ray microscope. A proposed modeling method was used to obtain an optimal design, which was verified with a finite element analysis. The fine positioner was then constructed and an experiment was used to validate its performance.

Manuscript received: March 4, 2005 / Accepted: January 17, 2006

1. Introduction

With the rapid developments in biology and engineering, the need for microscopes with high magnification and resolution has increased. Microscopes can be categorized into optical microscopes and electron microscopes, depending on their light source. Optical microscopes, which use visible light, can observe living specimens and are easy to handle, but their resolution is limited by the wavelength of the light source. Electron microscopes use electrons as a light source to improve their resolution, which can be in the sub-nanometer range. However, the transmissibility of electron beams through biological specimens is so low that specimens must be preprocessed; they are usually cryofixed and sliced. This prevents us from observing living specimens. In addition, electron beams can damage the specimens.

To overcome these problems, X-ray microscopes have been researched around the world. The wavelength of X-rays ranges from 0.1 to 30 nm, so that image resolutions in the nanometer range can be obtained. X-rays also have high transmissibility, so that biological samples do not need to be preprocessed; they can be observed in a thick and living state. In addition, the absorption coefficients of X-rays are highly related to the atomic number of matter, so that they can be widely used to observe bio-samples.

There are several ways in which the optics of an X-ray microscope can be set up. Fig. 1 shows the X-ray microscope considered in this paper, which used transmission optics. A 1:1 double ellipsoid mirror acted as a condenser to illuminate the specimen and a 1000:1 zone-plate provided the objective optics. The condenser and objective were aligned separately. These optics were designed to obtain a high level of magnification; therefore, the alignment of the optical components was important. In particular, the condenser mirror must be aligned with 5 degrees-of-freedom (DOF), from which rotation about the optic axis is excluded.

The overall image quality is highly dependent on the alignment and vibration of the condenser. So far, however, little research has been directed towards the alignment of the condenser mirror in an X-ray microscope. X-ray microscopes have been constructed and tested in a number of studies, but the alignment of the optics has not been discussed.[1-5] Voss listed the types of optics used in X-ray microscopes and referred to the importance of their alignment.[6] It has also been stated that the precision required for aligning the optics depends on the type of optics.[7,8] Matyi *et al.* suggested a method for aligning crossed parabolic X-ray mirrors, but it requires manual lead screws that cannot be used for precise alignments.[9] Therefore, the precise alignment required for the optics in an X-ray microscope has seldom been studied. A fine positioner with more than 5 DOF and high stiffness and resolution values is required. Such a positioner is proposed, modeled, constructed, and tested in this paper.

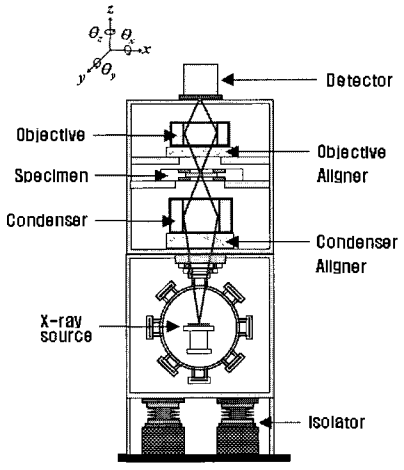

Fig. 1 Schematic diagram of an X-ray microscope

2. Concept design for the fine positioner

The DOF required by an optics aligner in an X-ray microscope depends on the type of optics, but generally at least 5 DOF must be used. Fine positioners with more than 5 DOF can be categorized as serial linkage or parallel linkage mechanisms by the type of connection actuator used between the base and end-effector. A concept diagram of serial and parallel linkage mechanisms is depicted in Fig. 2. In general, serial linkage mechanisms have large workspaces and simple forward kinematics, while parallel linkage mechanisms are smaller and have high stiffness values, no error accumulation in the end-effector actuator, and simple inverse kinematics. Since the desired optics aligner should be stiff and small, a parallel linkage mechanism was adopted in this study.

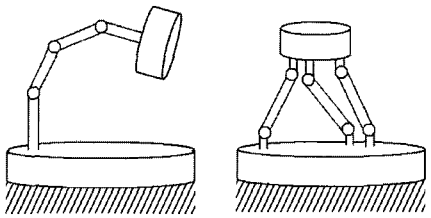

Fig. 2 (a) Serial and (b) parallel linkage mechanisms

The most typical parallel linkage mechanism with more than 5 DOF is a Stewart platform, which is depicted in Fig. 3. Each strut must have 6 DOF if the Stewart platform is to have 6 DOF. This can be realized using a ball joint (3 DOF) and a universal joint (2 DOF) in each strut. The additional 1 DOF is provided by the linear motion of the linear motor because it can be actuated freely. These types of rotational joints have been used in Stewart platforms with large workspaces. However, they introduce friction and clearance requirements that cause backlash and make it impossible to obtain high resolutions. Therefore, a new type of rotational joints is required.

Fig. 4 shows the concept of a cylindrical flexure. It has 3 rotational DOF, similar to a ball joint, so that each strut of the Stewart platform will have 7 DOF if the flexure is used at both ends of the strut. This will give a Stewart platform with 12 DOF. However, 6 of these DOF are the rotation of struts, which do not influence the position of the end-effector. Therefore, the end-effector can be positioned with 6 DOF using six linear motors.

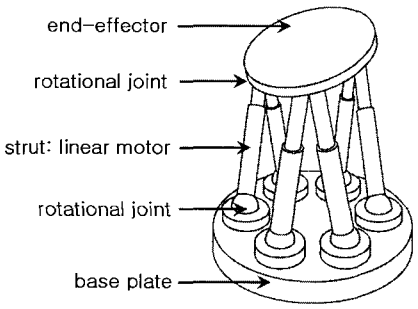

Fig. 3 Schematic diagram of a Stewart platform

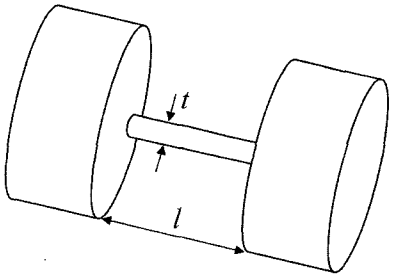

Fig. 4 Concept diagram of a cylindrical flexure

3. Modeling the Stewart platform with flexures

Ryu[10] and Kang[11] have modeled a flexure hinge mechanism, which can be considered a spring-mass system. The total potential and kinetic energy are calculated from the parameters of the mechanism and the equation of motion can be derived from Lagrange's equation. This process is shown in Fig. 5. This modeling method was modified so it could be applied to a cylindrical flexure mechanism.

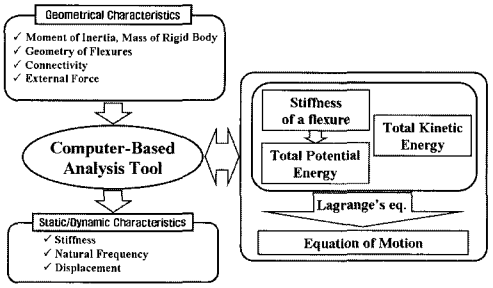

Fig. 5 Modeling the flexure mechanism

Consider the spring-mass system described by Fig. 6. The potential energy stored in the k^{th} flexure spring connecting the i^{th} and j^{th} rigid bodies is

$$V_k = \frac{1}{2}\begin{bmatrix} u_T^{\,k} \\ u_R^{\,k} \end{bmatrix}^T k^k \begin{bmatrix} u_T^{\,k} \\ u_R^{\,k} \end{bmatrix} \tag{1}$$

where $u_T^{\,k}$ and $u_R^{\,k}$ are vectors that represent the translational and rotational deformations of the k^{th} flexure spring, respectively, and k^k is the stiffness matrix of the k^{th} flexure spring. Let us denote the connectivity points of the flexure on bodies i and j as p^i and q^j, and their displacements as u_{pi} and u_{qj}, respectively. Then $u_T^{\,k}$ and $u_R^{\,k}$ can be written as

$$\begin{aligned} u_T^{\,k} &= u_{p^i} - u_{q^j} \\ u_R^{\,k} &= \Theta^i - \Theta^j \end{aligned} \tag{2}$$

where Θ^i and Θ^j represent the orientation of the i^{th} and j^{th} bodies. The stiffness matrix of the k^{th} flexure spring can be written as

$$k^k = R^k k_h^{\,k} R^{k^T} \tag{3}$$

where $k_h^{\,k}$ is the stiffness matrix of the k^{th} flexure spring with respect to the flexure coordinates system depicted in Fig. 7, which can be written as

$$k_h^{\,k} = \begin{bmatrix} \frac{\partial \Delta x}{\partial F_x} & 0 & 0 & 0 & 0 & 0 \\ 0 & \frac{\partial \Delta y}{\partial F_y} & 0 & 0 & 0 & \frac{\partial \Delta y}{\partial M_z} \\ 0 & 0 & \frac{\partial \Delta z}{\partial F_z} & 0 & \frac{\partial \Delta z}{\partial M_y} & 0 \\ 0 & 0 & 0 & \frac{\partial \Delta \alpha}{\partial M_x} & 0 & 0 \\ 0 & 0 & \frac{\partial \Delta \beta}{\partial F_z} & 0 & \frac{\partial \Delta \beta}{\partial M_y} & 0 \\ 0 & \frac{\partial \Delta \gamma}{\partial F_y} & 0 & 0 & 0 & \frac{\partial \Delta \gamma}{\partial M_z} \end{bmatrix}^{-1} \tag{4}$$

and R^k is a transformation matrix used to convert from the flexure coordinate system to the global coordinate system. Each component

in Equation (4), which is a function of the diameter and length of the cylindrical flexure, can be calculated from the fundamental equations for tension, bending, and torsion in material engineering. The total potential energy of the mechanism can be obtained by summing all the potential energies of the flexure springs,

$$\begin{aligned} V = \sum_{k=1}^{N_s} \frac{1}{2} \Big[& q^{i^T} T_p{}^{i^T} R^k k_h{}^k R^{k^T} T_p{}^i q^i \\ & - q^{i^T} T_p{}^{i^T} R^k k_h{}^k R^{k^T} T_p{}^j q^j \\ & - q^{j^T} T_p{}^{j^T} R^k k_h{}^k R^{k^T} T_p{}^i q^i \\ & + q^{j^T} T_p{}^{j^T} R^k k_h{}^k R^{k^T} T_p{}^j q^j \ \Big] \end{aligned} \tag{5}$$

where N_s is the number of flexure springs and T, which contains information about p^i and q^j in flexure coordinates, can be described as

$$\begin{aligned} \begin{bmatrix} u_T{}^k \\ u_R{}^k \end{bmatrix} &= T_p{}^i q^i - T_q{}^j q^j \\ q^i &= \begin{bmatrix} dr^i \\ \Theta^i \end{bmatrix} \end{aligned} \tag{6}$$

where dr^i is the translation vector of the i^{th} body.

The kinetic energy of the i^{th} rigid body is the sum of the translational and rotational kinetic energies, which can be written as

$$T^i = \frac{1}{2} d\dot{r}^T m^i d\dot{r} + \frac{1}{2} \dot{\Theta}^{i^T} j^i \dot{\Theta}^i \tag{7}$$

where m^i is the mass matrix of the i^{th} body and j^i is the central inertia tensor with respect to the body-fixed coordinates system of the i^{th} body, which is assumed to be located at the center of mass of the i^{th} body,

$$\begin{aligned} m^i &= diag\left[m^i, m^i, m^i \right] \\ j^i &= diag\left[I_x{}^i, I_y{}^i, I_z{}^i \right] \end{aligned} \tag{8}$$

The total kinetic energy of the mechanism is obtained by summing all the kinetic energies of the rigid bodies,

$$T = \sum_{i=1}^{N_b} T^i = \sum_{i=1}^{N_b} \frac{1}{2} \dot{q}^{i^T} M^i \dot{q}^i \tag{9}$$

where

$$\begin{aligned} M^i &= \begin{bmatrix} m^i & 0 \\ 0 & j^i \end{bmatrix} \\ q^i &= \begin{bmatrix} dr^i \\ \Theta^i \end{bmatrix} \\ N_b &= number \quad of \quad bodies \end{aligned} \tag{10}$$

The method of modeling the cylindrical flexure mechanism was verified by comparing the results using the proposed model and a finite element model (FEM). The flexure jointed Stewart platform shown in Fig. 8 was tested. All the calculations assumed that the actuators were fixed, so that the Stewart platform actually had no mobility because once the condenser mirror is aligned, it is fixed at that position.

Table 1 shows the stiffness of the test structure calculated using the proposed model and the FEM. The differences between the values were less than 10%. Table 2 compares the natural frequencies obtained from the two models. Vibrations in the struts occur when the end-effector is almost stationary. Table 2 also indicates that the discrepancies between the two models were within 10%. The discrepancies in Tables 1 and 2 were caused by assuming that the bodies were rigid in the proposed model, while they were flexible in the FEM.

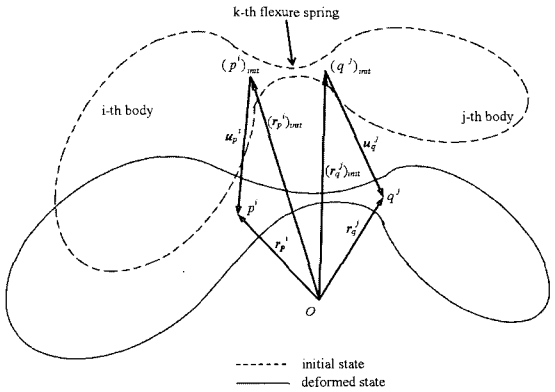

Fig. 6 k^{th} flexure spring connecting the i^{th} and j^{th} rigid bodies

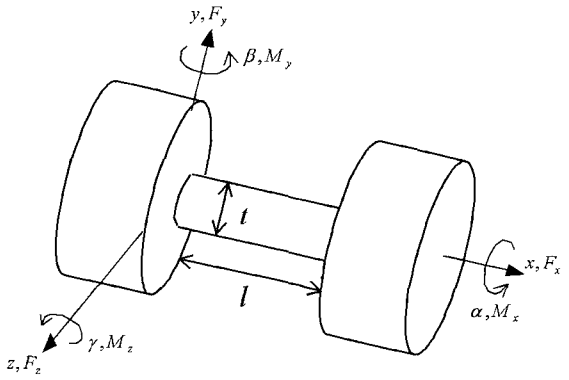

Fig. 7 Flexure coordinate system

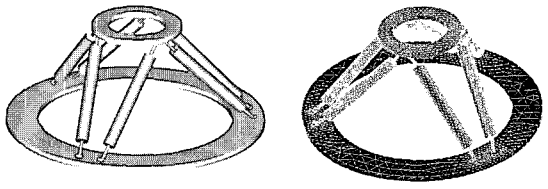

Fig. 8 Test structure used to verify the cylindrical flexure model

Table 1 Stiffness of the Stewart platform in the proposed model and the FEM

Stiffness (N/um)	K_x	K_y	K_z
Proposed Model	105.6	105.6	249.4
FEM	99.0	99.0	230.4
Stiffness (Nm/mrad)	$K_{\theta x}$	$K_{\theta y}$	$K_{\theta z}$
Proposed Model	105.6	105.6	249.4
FEM	99.0	99.0	230.4

Table 2 Natural frequencies of the Stewart platform obtained from the proposed model and the FEM

Vibration mode	Vibration of the end-effector (Hz)		
	$x+\theta_y$	z	θ_z
Proposed Model	698	752	743
FEM	658	699	710
Vibration mode	Vibration of the struts (Hz)		
	rotation	translation (1)	translation (2)
Proposed Model	712	756	764
FEM	703	731	745

4. Optimal design of the Stewart platform

An optimal design is required to maximize the performance of the Stewart platform. The most important characteristic of a condenser mirror aligner in an X-ray microscope is its robustness, *i.e.*, high stiffness. Therefore, the objective function is

$$minimize \quad \sum_i \frac{1}{\omega_i^2} \tag{11}$$

where ω_i represents the natural frequencies of the first-order vibration modes shown in Table 2.

There are seven design variables:

- the length and diameter of the cylindrical flexure (2),
- the height of the Stewart platform,
- the radius and shape of the base plate (2), and
- the radius and shape of the end-effector (2).

The last four variables are illustrated in Fig. 9. The vertices are the connection points between the struts and base plate or end-effector. The base plate and end-effector are symmetric, so that the Stewart platform is robust to thermal deformation.

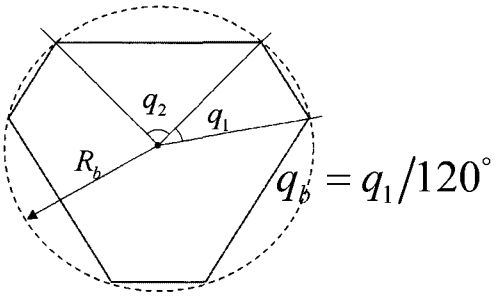

Fig. 9 Radius and shape of the base plate and end-effector

There are six constraints:

- the workspace of the end-effector should be greater than

$$\begin{aligned} -0.2 \le x, y, z \le 0.2(mm) \\ -3.5 \le \theta_x, \theta_y, \theta_z \le 3.5(mrad) \end{aligned} \tag{12}$$

- the maximum stress on the cylindrical flexures should be less than 20% of the yield stress of the material,
- the end-effector should be smaller than the base plate to ensure structural stability,
- there must be no singularities in the workspace of the end-effector,[12]
- the lower and upper boundaries of the design variables must be observed, and
- there must be no interference in the assembly.

Sequential quadratic programming (SQP) was used to obtain the optimal design. This algorithm does not guarantee a global minimum of the objective function. Therefore, several starting points were tested. Fig. 10 and Table 3 show the convergence of the objective function and the results of the global minimum verification. The variables listed in Table 3 are the global optimal values.

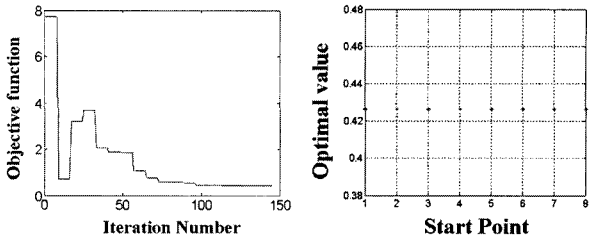

Fig. 10 Optimal values for several starting points

Table 3 Optimal values for several starting points

variables	starting points				optimal
t (mm)	1	5	3	2	2.51
l (mm)	10	25	13	13	25
R_b (mm)	150	250	200	220	209.21
R_t (mm)	60	150	100	90	60
h (mm)	150	150	200	180	200
q_b	0.1	0.1	0.3	0.15	0.1
q_t	0.2	0.2	0.5	0.6	0.584

5. Experiment using the Stewart platform

Based on the optimal design results, a Stewart platform was constructed, as shown in Fig. 11. The linear motors were the 2000DC series from Diamond Motion. The other parts, including the cylindrical flexures, were manufactured and assembled. The experiment consisted of measuring the resolution and workspace, and confirming the kinematics. The motion of the end-effector was measured using a hexahedron block and six proximity sensors, as shown in Fig. 12. The numbered cylinders were the sensor probes. The position and pose of the end-effector can be determined in this way. For example, the translation of the end-effector in the y direction was measured by averaging the measurements of probes 1 and 2, while the rotation about θ_x was calculated by dividing the difference between the measurements of probes 1 and 2 by the distance between the two probes. The positions and poses of the end-effector in other directions can be determined in a similar manner.

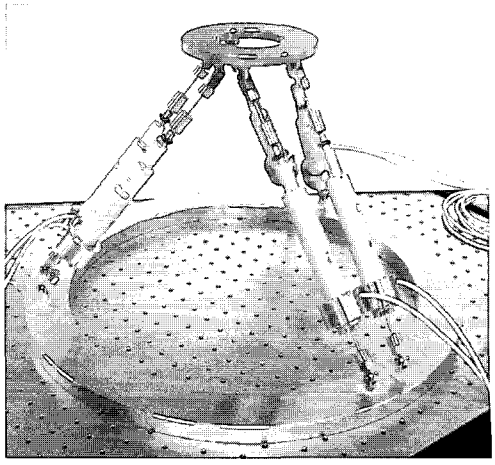

Fig. 11 Constructed Stewart platform

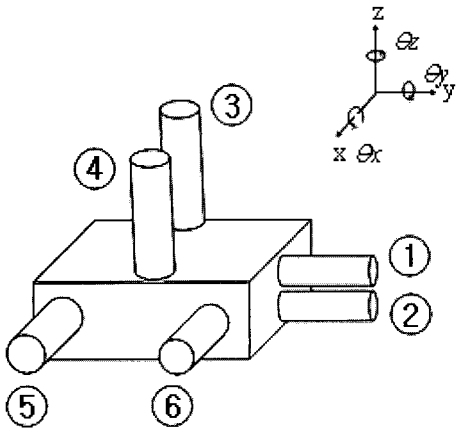

Fig. 12 Measurement system for the end-effector

Fig. 13 shows the resolution measurements. The translational resolution was 50 nm in the x, y, and z directions while the rotational resolution was 7.3, 3.9, and 0.97 μrad in the θ_x, θ_y, and θ_z directions, respectively. The rotational resolution was determined from the distance between probes measuring the same surface. This explains why the rotational resolutions were different from each other. All the resolutions were limited by the electrical noise of the proximity sensors. Fig. 14 shows the workspace measurements and confirms that the optimal design was used.

Fig. 15 shows the results of the inverse kinematics. The end-effector of the Stewart platform was moved to the positive and negative limit points in each direction, where the position and pose of end-effector were measured. For example, in the uppermost two plots, the translations of the end-effector are shown on the left-hand side while the rotations are shown on the right-hand side. When the end-effector was moved to its positive limit point, *i.e.*, 0.2 mm, the movements in the other directions were less than 10% of their own limits. The lower plots were measured in the same manner. These results confirm that the inverse kinematics of the Stewart platform had errors of less than 10%. These errors were caused by the manufacturing, assembly, and measurement processes.

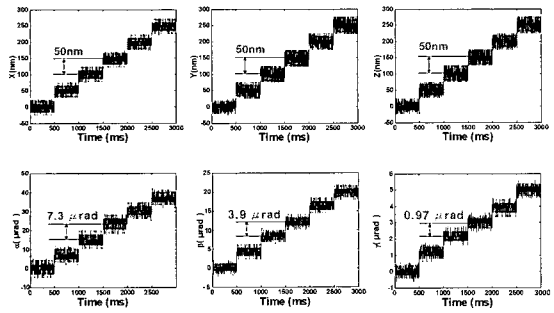

Fig. 13 Resolution measurement results

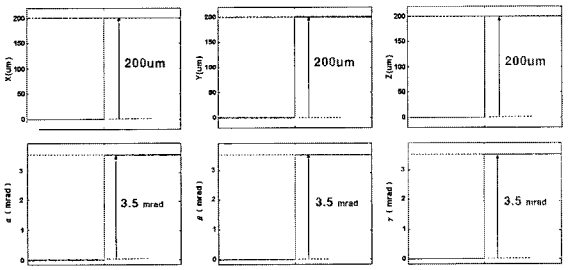

Fig. 14 Workspace measurement results

6. Conclusions

The condenser mirror in an X-ray microscope must be aligned precisely in 5 DOF and must maintain that position. This requires a high-resolution, high-stiffness mechanism with more than 5 DOF. A Stewart platform was adopted for this task because of its DOF and high level of stiffness. Cylindrical flexures were used for the joints of the Stewart platform to overcome the backlash and friction problems. The entire flexure mechanism was modeled mathematically. The modeling was verified by comparing the results with those obtained from an FEM. Based on the mathematical modeling, the design variables of the mechanism were optimized to maximize the natural frequency.

The Stewart platform was constructed and tested. The tests consisted of resolution and workspace measurements, as well as a verification of the inverse kinematics. The tests showed that the mechanism had a 50-nm resolution in the x, y, and z directions, and 7.3-, 3.9-, and 0.97-μrad resolution in the θ_x, θ_y, and θ_z directions, respectively. A designed workspace with 200 μm of translation and 3.5 mrad of rotation was also measured. The inverse kinematics test demonstrated that the mechanism had an inverse kinematics error of less than 10%.

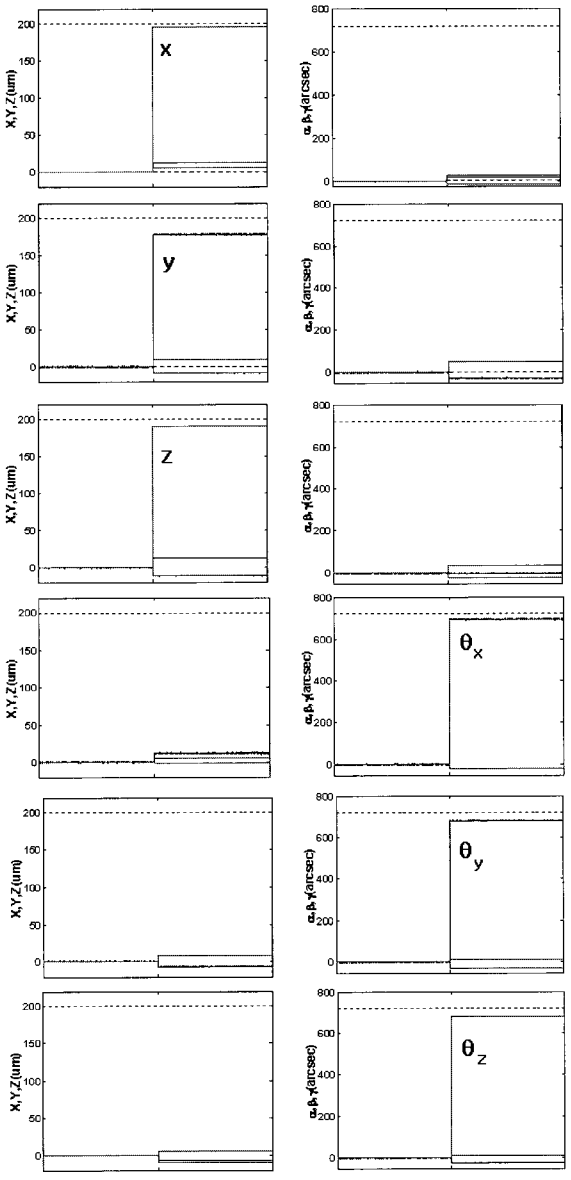

Fig. 15 Confirmation of the inverse kinematics

REFERENCES

1. Takeuchi, A., Aoki, S., Yamamoto, K., Takano, H., Watanabe, N. and Ando, M., "Full-field x-ray fluorescence imaging microscope with a Wolter mirror," Review of Scientific Instruments, Vol. 71, No. 3, pp. 1279-1285, 2000.

2. Ninomiya, K. and Hasegawa, M., "Scanning photoelectron microscope with submicron lateral resolution using a Wolter-type x-ray focusing mirror," Journal of Vacuum Science Technology A, Vol. 13, No. 3, pp. 1224-1228, 1995.

3. Watanabe, N., Yamamoto, K., Takano, H., Ohigashi, T., Yokosuka, H., Aota, T. and Aoki, S., "X-ray fluorescence microtomography with a Wolter mirror system," Nuclear Instruments and Methods in Physics Research A, Vol. 467-468, No. 2, pp. 837-840, 2001.

4. Aoki, S., Kumegawa, M., Watanabe, N., Ohigashi, T., Aota, T., Yamamoto, K., Yokosuka, H., Tanoue, R., Tsujita, Y. and Anto, M., "X-ray scattering microscope with a Wolter mirror," Review of Scientific Instruments, Vol. 73, No. 7, pp. 2629-2633, 2002.

5. Hasagawa, M., Yoneyama, A. and Ninomiya, K., "Soft x-ray scanning photoelectron microscope using Wolter-type focusing mirror," Journal of Electron Spectroscopy and Related Phenomena, Vol. 80, pp. 361-364, 1996.

6. Voss, J., "The scanning soft X-ray microscope at Hasylab: imaging and spectroscopy of photoelectrons, photoluminescence, desorbed ions, reflected, scattered and transmitted light," Journal of Electron Spectroscopy and Related Phenomena, Vol. 84, No. 1/3, pp. 29-44, 1997.

7. Horikawa, Y., "Consideration on the condenser for an imaging type Schwarzschild soft X-ray microscope," Journal of Modern Optics, Vol. 40, No. 2, pp. 289-298, 1993.

8. Berglund, M., Rymell, L., Peuker, M., Wilhein, T. and Hertz, H. M., "Compact water-window transmission X-ray microscope," Journal of Microscopy, Vol. 197, pp. 268-273, 1999.

9. Matyi, R. J., Moran, P. D., Hagquist, W. W. D. and Volz, H. M., "Alignment system for crossed parabolic x-ray mirrors," Review of Scientific Instruments, Vol. 71, No. 6, pp. 2292-2295, 2000.

10. Ryu, J. W., "6-Axis ultraprecision positioning mechanism design and positioning control," Ph.D. dissertation, KAIST, Daejon, South Korea, 1997.

11. Kang, D. W., "The design and test of ultraprecision XY stage using leaf spring mechanism and voice-coil motor," Masters dissertation, KAIST, Daejon, South Korea, 1997.

12. Mohammadi Diniali, H. R., Zsombor-Murray, P. J. and Angeles, J., "Singularity analysis of planar parallel manipulators," Mech. Mach. Theory, Vol. 30, No. 5, pp. 665-678, 1995.